Waipapa Taumata Rau
University of Auckland

Flow Rate from a Longitudinal Split in a PVC pipe, McCrae

17 July 2025

Flow Rate from a Longitudinal Split in a PVC pipe, McCrae

Authors

Dr Jakobus E van Zyl

Dr Andrew Brown

Date

17 July 2025

Contents

Figures

Tables

1 Introduction

1.1 Background

South East Water (SEW) identified and repaired a burst water main on 30 December 2024, adjacent to a heavily vegetated area. Subsequent zone flowmeter analysis by SEW estimated that the burst started as a small flow at approximately 1 November 2024. This period coincided with reports of groundwater surfacing downhill of the burst site. SEW required an analysis of the water flow from the pipe to the ground surface.

1.2 Project Objectives

The project objectives were to explain, characterise and calculate the following over the flow range/period:

1. Flow rate relationship from the burst pipe.
2. Soil interaction with water leaving the pipe, including soil fluidisation, saturation zone and soil transport to the surface.
3. The quantity of water from the pipe that reached the ground surface.
4. Longitudinal split size growth.

1.3 Layout of this Report

The body of this report is presented in three sections:

- Section 2: The development of the split over time.
- Section 3: A description of soil-leak interaction outside pipes.
- Section 4: The leakage flow reaching the ground surface.

2 Longitudinal Pipe Split

Longitudinal splits are a common failure type found in uPVC pipes since the main pipe wall stresses due to internal pressure are in a circumferential direction. Longitudinal splits are often caused by fatigue cracking due to diurnal and transient pressure fluctuations.

This section provides background material on fatigue cracking, leakage flow behaviour and relevant laboratory leak flow results. It then analyses the McCrae pipe split to estimate the development of the split length over time.

2.1 Background

2.1.1 Fatigue Crack Modelling

Material fatigue in pipes is caused by pressure cycles and contributes significantly to the development and growth of pipe cracks. (Note that this report uses 'crack' and 'split' synonymously.) Crack initiation due to fatigue happens at a microscopic level and is influenced by the pressure load, number of loading cycles, and microstructure of the material (Bardet et al. 2010; Rajani and Kleiner 2012; Richard and Sander 2016).

Crack propagation occurs through a cumulative fracture process in which the crack grows incrementally due to fluctuating load cycles. Once the crack reaches a critical length, residual fracture occurs, causing rapid catastrophic failure of the pipe.

Crack propagation due to pressure fatigue is modelled using the Paris law, which is based on fracture mechanics principles:

$$\frac{da}{dN} = C_1 \, \Delta K^{C_2} \tag{1}$$

Where a is half the crack length (m), N the number of cycles, ΔK the stress intensity factor in (MPa $\sqrt{m}$), and C_1 (in $\frac{m/cycle}{(MPa\sqrt{m})^m}$) and C_2 (-) are material-dependent constants. The stress intensity factor is given by the equation:

$$\Delta K = \Delta P \frac{D}{2t} Y \sqrt{\pi a} \tag{2}$$

Where ΔP is the size of the pressure fluctuation (MPa), D pipe diameter (m), and t wall thickness (m). Y is a geometric factor based on the crack length, pipe diameter and wall thickness.

Fatigue fracture is not driven by the maximum pipe pressure, but by the size of pressure fluctuations, the number of cycles, and the current crack length. Pipes are subjected to several pressure fluctuations, including diurnal, background transient noise and large transients, all of which may contribute to crack growth.

Plastic pipes are flexible but can deteriorate and become more brittle, for instance, due to UV light exposure, cold temperatures, disinfectants, hydrocarbons, and solvents (Barton et al., 2019; Brandt et al., 2017). Crack growth rates in PVC are significantly affected by the additives used in the manufacturing process (Farrow et al. 2017).

2.1.2 Leakage Flow Modelling

Leaks are hydraulic orifices and thus adhere to the orifice equation derived from the Conservation of Energy principle. The orifice equation for the flow rate Q through an orifice or leak is given by:

$$Q = C_d A\sqrt{2gh} \tag{3}$$

Where C_d is the discharge coefficient, A leak area, g gravitational acceleration, and h pressure head.

It has been shown that the areas of leak openings are not fixed but vary linearly with pressure (Cassa and van Zyl 2013; Van Zyl and Malde 2017). Thus, the leak area can be described by:

$$A = A_0 + mh \tag{4}$$

Where A_0 is the initial leak area (under zero pressure conditions), and m the head-area slope. Replacing this equation in the orifice equation results in the modified orifice or FAVAD (Fixed and Variable Area Discharges) equation:

$$Q = C_d\sqrt{2g}(A_0 h^{0.5} + m\, h^{1.5}) \tag{5}$$

The modified orifice equation consists of two terms that vary with pressure to the power of 0.5 and 1.5, respectively. Van Zyl et al. (2017) discuss the modified orifice equation and its implications for leakage behaviour.

The head-area slope m is determined by the leak type (e.g. round hole, longitudinal crack or circumferential crack), leak dimensions, and pipe material, diameter and wall thickness. In general, the head-area slopes of longitudinal splits are much greater than those of round holes or circumferential cracks.

Three theoretical models for predicting the head-area slope of longitudinal splits in pipes have been proposed: the empirical Cassa and Fox equations, and the Tada-Paris model. The Tada-Paris model was developed from basic fracture mechanics principles and is thus preferred and used in this study.

Cassa Equation

Cassa and van Zyl (2013) proposed an empirical equation based on the results of finite element analysis of the variation of longitudinal crack area with pressure:

$$m_{longitudinal} = \frac{2.93157\, D^{0.3379}\, L_C^{4.8} 10^{0.5997(log L_c)^2}\, \rho\, g}{E\, t^{1.746}} \tag{6}$$

Where *D* is the pipe diameter (m), L_c crack length (m), E elasticity modulus (Pa), t wall thickness (m), and ρ water density (kg/m^3).

Fox Equation

The Fox equation (Fox et al., 2018) is a semi-empirical model that describes changes in longitudinal split area in PE pipes. It can be applied to other materials but is less accurate than the Cassa and Tada-Paris methods. The change in the leak area *dA* is given by:

$$dA = C\frac{p}{E}\frac{L_c^4}{t^2} \tag{7}$$

$$C = 0.0065\left(\frac{\pi D}{L_c}\right) + 0.2315 \tag{8}$$

Where D is the pipe diameter, L_c crack length, E elasticity modulus, and t wall thickness.

Tada-Paris Method

The analytical Tada-Paris method was developed from basic materials science principles for thin-walled pressure vessels, defined as a radius/wall thickness ratio ≥ 10 (Paris and Tada, 1983).

Estimating leak opening area for longitudinal cracks in internal pressure loading involves calculating a stress intensity factor (K_l), which is a function of the geometric parameter (λ) and determines the severity of the crack. The stress intensity factor (K_l) for a longitudinal crack of length $2a$ is given by:

$$K_l = \sigma_h\sqrt{\pi a}\, F_l(\lambda) \tag{9}$$

Where F_l is the geometric factor for longitudinal cracks and σ_h the circumferential stress, which is a function of the pressure, pipe diameter and wall thickness. The geometric parameter (λ), which relates to the pipe inner radius (R), pipe wall thickness (t) and crack length $(2a)$, is given as:

$$\lambda = \frac{a}{\sqrt{Rt}} \tag{10}$$

The geometric factor for longitudinal cracks $F_l(\lambda)$ is calculated as a function of a geometric parameter (λ) as (Rooke and Cartwright, 1976):

$$F_l(\lambda) = \begin{cases} (1 + 1.25\lambda^2)^{0.5}\,; (0 \le \lambda \le 1) \\ 0.6 + 0.9\lambda; (1 \le \lambda \le 5) \end{cases} \tag{11}$$

The leak opening area for longitudinal cracks subjected to internal pressure loading is:

$$A_l = \frac{\sigma_h}{E}(2\pi Rt)G_l(\lambda) \tag{12}$$

Where $G_l(\lambda)$ is evaluated as:

$$G_l(\lambda) = \begin{cases} \lambda^2 + 0.625\lambda^4\,; (0 \le \lambda \le 1) \\ 0.14 + 0.36\lambda^2 + 0.72\lambda^3 + 0.405\lambda^4\,; (1 \le \lambda \le 5) \end{cases} \tag{13}$$

The head-area slope for longitudinal cracks can be expressed, independent of pressure, as follows:

$$m = \begin{cases} \frac{\rho g}{E}(6.283Ra^2t^{-1} + 3.927a^4t^{-2})\,; 0 \le \lambda \le 1 \\ \frac{\rho g}{E}(0.879R^2 + 2.260a^2Rt^{-1} + 4.524a^3R^{0.5}t^{-1.5} + 2.545a^4t^{-2}); 1 \le \lambda \le 5 \end{cases} \tag{14}$$

2.1.3 Relevant Laboratory Results

The University of Auckland recently conducted an extensive laboratory study consisting of 126 experimental tests on leaks in water distribution pipes with a range of leak types (round hole, longitudinal slit, circumferential slit), sizes (small, medium, large), pipe materials (steel, PVC, PE), pipe diameters (50, 100, and 200 mm) and wall thicknesses (classes PN6, PN9, and PN12).

The most relevant tests to this study are the 100 and 200 mm longitudinal splits in 100 and 200 mm

diameter Class 12 uPVC pipes. The properties of these pipes and their measured discharge coefficients (C_d) and head-area slopes (m) are summarised in Table 1.

Table 1 Experimental discharge coefficients (C_d) and head-area slopes (m) obtained for longitudinal slits in uPVC pipes

Nominal diameter (mm)	Outer diameter (mm)	Wall thickness (mm)	Split length (mm)	C_d	m (mm²/m)
100	114.3	7	100	0.62	1.8
100	114.3	7	200	0.60	20.5
200	225.3	12.3	100	0.62	1.8
200	225.3	12.3	200	0.64	15.2

2.2 McCrae Pipe Split

2.2.1 Pipe and Split Properties

The split occurred on a 150 mm nominal diameter uPVC Class 12 pipe installed in 1963 at a depth of 1.7 m. The static pressure at the split is 73 m with a minimum diurnal value of 70 m.

No photographs or measurements of the split are available, but the maintenance records describe it as a longitudinal split. The repair crew reported several weeks after the repair that the split was approximately 100 mm long and at a position of 4 o'clock.

The discharge coefficient C_d was assumed to be 0.65, a typical value for longitudinal splits.

ExcelPlas (2025) conducted a detailed condition analysis on a section of an identical main taken from near the location of the split. They measured the mean outer diameter and wall thickness as 168.7 mm and 9.1 mm, respectively.

ExcelPlas also reported the average elasticity modulus of the pipe material at positions of 6 and 12 o'clock to be 3.873 GPa and 4.045 GPa, respectively. The average of these two values, 3.959 GPa, was used in this study. This is significantly higher than the range of 2 – 4 GPa normally listed for uPVC.

2.2.2 Leakage Flow Rate Analysis

The water lost through the leak was estimated by SEW through a mass balance of flow meters and compensating for typical water consumption patterns (Crook, 2025) and is shown in Fig. 1. The report notes that, while there are short term fluctuations in the data around zero, there is a distinct and consistent increase of flow indicating the split development until it reaches a maximum on 30/12/24, after which it was repaired on 31/12/24. SEW identifies two possible starting dates for the leak:

- 05/10/24, the leak ran for 85 days with an estimated total loss of 34 to 41 ML.
- 30/10/24, the leak ran for 60 days with an estimated total loss of 34 to 39 ML.

The daily leakage flow in Fig. 1 was assumed to be correct in this analysis.

The cumulative flow (or leakage volume) over time was calculated and is shown in Fig. 2. The cumulative flow graph is helpful as it removes data fluctuations and facilitates the identification of changes in the flow behaviour. The cumulative flow graph initially shows a fluctuation around zero, which is expected for a system without leaks. However, the cumulative outflow became positive

around 3/8/2024, indicating that the split may have been initiated on this date. This is shown in more detail in Fig. 3.

A careful study of the cumulative flow graph identified changes in the slope of the leak volume line that likely correspond to changes in the split length. Periods with similar behaviour were identified, and suitable curves were fitted to them, as shown in Fig. 4.

Finally, the first derivatives of the cumulative flow curves were used to obtain the daily flow rate, and then plotted on the flow data in Fig. 5. The flow shows abrupt increases, which are consistent with sudden increases in the crack length as part of the fatigue fracture process. These increases may have been triggered by transient pressure waves due to pump stops and starts, or sudden valve changes.

The total leakage volume is estimated as 40.3 ML, close to the upper boundary estimated by SEW.

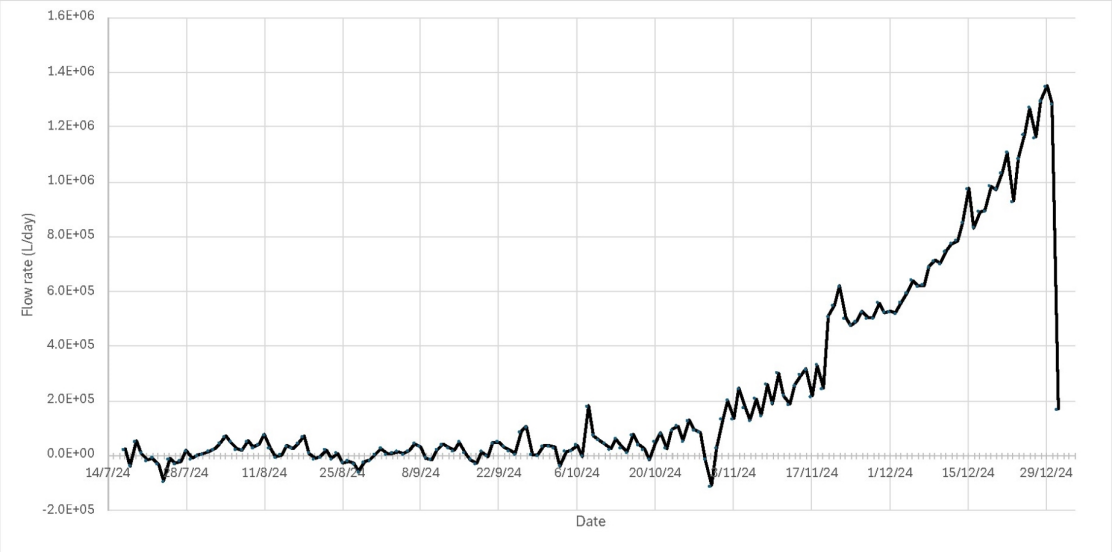

Figure 1 Measured leakage flow rate over time.

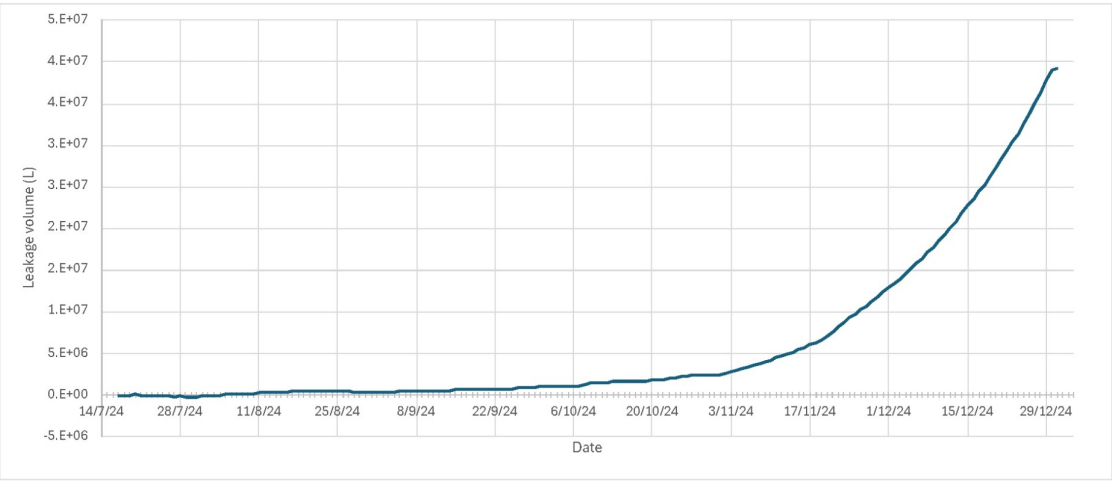

Figure 2 Cumulative flow (leakage volume) over time.

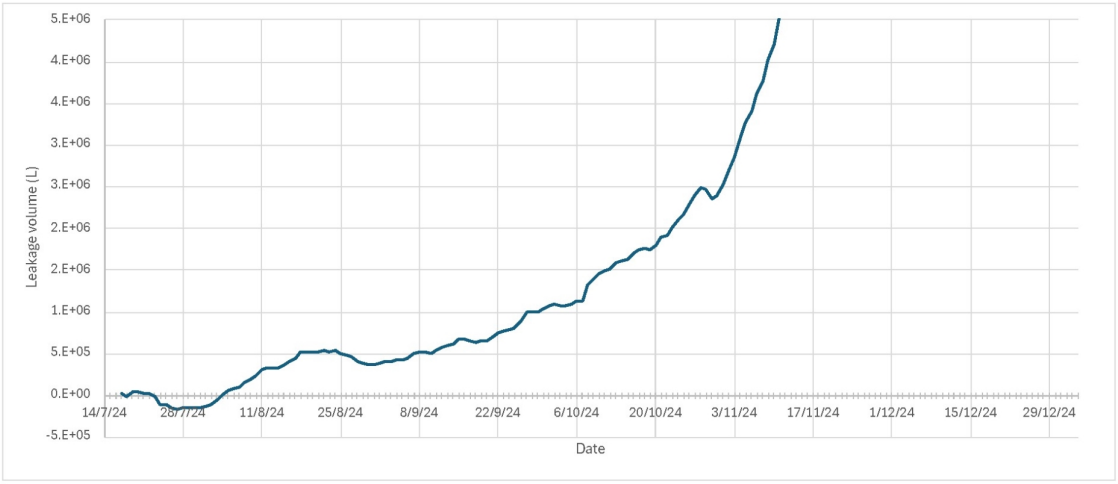

Figure 3 Cumulative flow (leakage volume) over time showing early detail.

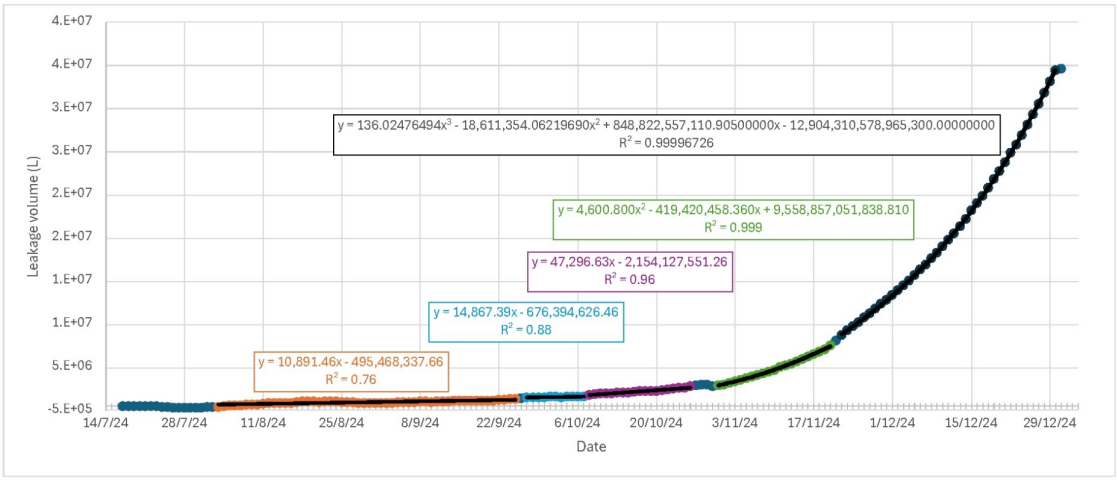

Figure 4 Models describing the leakage volume progression over time.

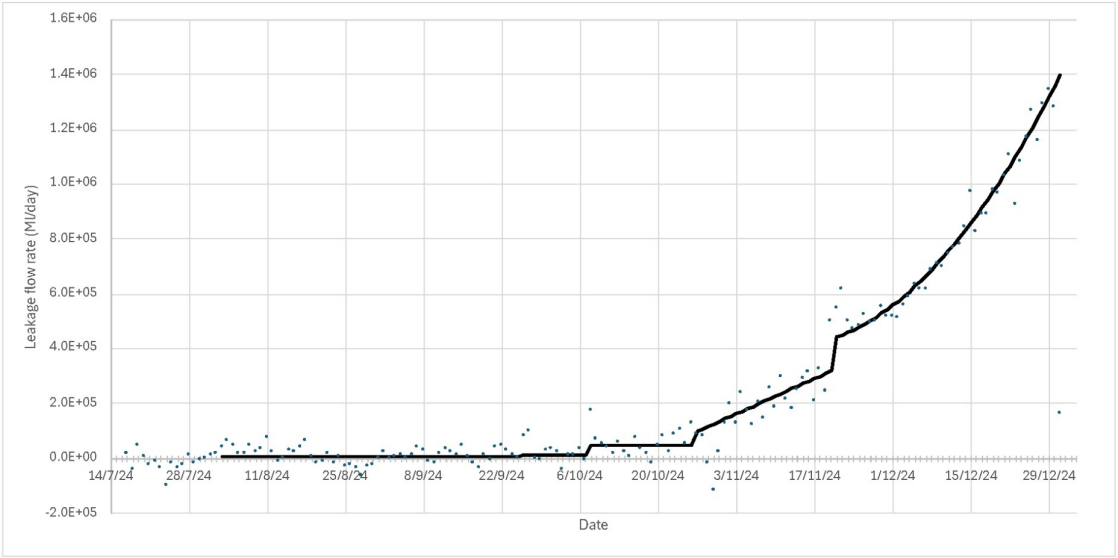

Figure 5 Modelled leakage flow rate over time.

2.2.3 Split Modelling

Model Calibration at Maximum Flow Rate

To model the dimensions and progression of the split, the modified orifice equation (Eq. 5) was first calibrated to the maximum flow rate of 1.397 ML/day reported for 30/12/24.

The initial area is determined by the split length and average width under zero-pressure conditions. Note that the calibration was done for the maximum split length (on 30/12/24) and does not consider the split growth over time. The terms 'initial area' and 'initial width' refer to the area and width of the maximum split length under zero-pressure conditions. Since the initial split width wasn't measured, it had to be assumed.

Very little research has been done on the dimensions of pipe failures. Beygi and Van Zyl (2024) conducted a pilot study, documenting leak dimensions from photographic records of one of the main maintenance contractors of Auckland, New Zealand. This study documented 32 longitudinal splits in PVC pipes, finding that the split length varied between 3 mm and 1,050 mm, with a mean value of 140 mm. Initial split widths varied between 0.1 mm and 20 mm, with a mean value of 2.2 mm. An initial split width of 2.2 mm was assumed for this study.

The remaining unknown parameter in the modified orifice equation is the head-area slope (m), which is a function of the split length (it is not significantly affected by the split width). The split head-area slope was estimated by calibrating the modified orifice equation to the maximum flow rate using a numerical solver.

The Tada-Paris model (Eqs. 9 – 14) was used to model the relationship between the head-area slope and split length. It is noted that the radius/width ratio of the pipe (8.3) is slightly below the required minimum value of 10 for the Tada-Paris equation. However, it is still expected to provide a reasonable estimate. The robustness of the results was tested against other models and experimental results, and using a sensitivity analysis.

A summary of the calibration calculation for a split width of 2.2 mm is provided in Table 2, showing an estimated maximum split length of 153 mm. This seems reasonable considering that the repair crew did not measure the split length but estimated it to be approximately 100 mm several weeks after the repair.

The head-area slope for the final split length was estimated using the Tada-Paris model as 4.57 mm^2/m. This seems reasonable compared to the measured head-area slopes of longitudinal splits in uPVC pipes listed in Table 1, especially when the higher-than-typical elasticity modulus of the pipe material is considered. The Cassa and Fox equations result in head-area slopes of 4.3 and 5.1 mm^2/m, respectively, providing further support for the reasonableness of the estimate.

Table 2 Calibration calculation summary for the split length at the maximum flow rate on 30/12/24.

Category	Parameter	Value
Pipe	External diameter (mm)	168.7
	Wall thickness (mm)	9.1
	Internal pipe diameter (mm)	150.5
	Modulus of elasticity (GPa)	3.959
System	Pressure head (m)	71.5
Split properties under zero-pressure conditions	Width (mm)	2.2
	Length (mm)	153
	A_0 (mm^2)	337.3
	C_d	0.65
	m (mm^2/m)	4.57
Pressurised split properties	Area (mm^2)	664.3
	Leak exit velocity (m/s)	37.5
	Leak flow rate (L/s)	16.2
	Leak flow rate (Ml/day)	1.397

Sensitivity of the Split Length to the Initial Split Width Assumption

A sensitivity analysis was done to evaluate the effect of the initial split width assumption by calibrating the leakage model for different initial widths. The result is shown in Fig. 6. A split length of 100 mm corresponds to a split width of 6 mm. On the other hand, an initial split width of zero corresponds to a split length of 187 mm. The assumed initial width of 2.2 mm seems reasonable, considering that an initial width of 6 mm is unlikely and the uncertainty associated with the split length estimate.

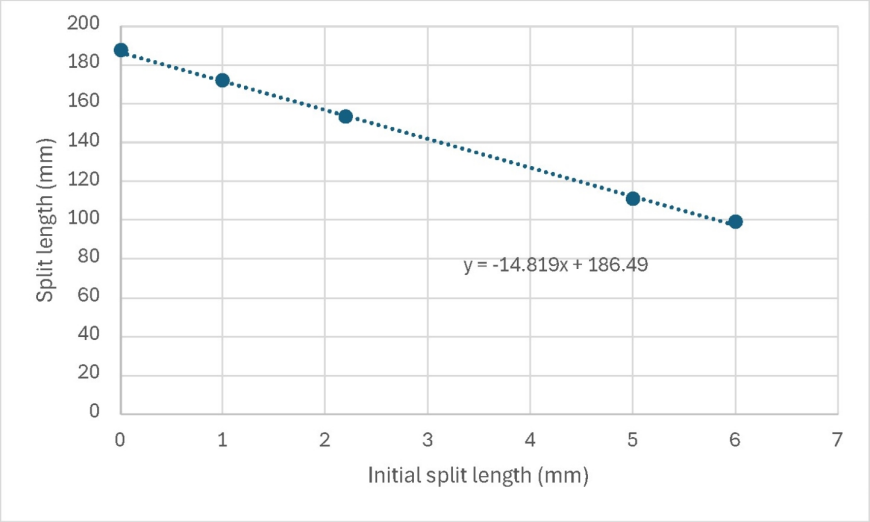

Figure 6 Calibrated split length as a function of assumed initial split width

Split Length Development Over Time

Once the modified orifice equation was calibrated to the maximum flow rate, it was possible to calculate the split length over time based on the flow rate in Fig. 5, assuming the split width to be proportional to its length. The results are shown in Fig. 7.

The figure shows that the split started abruptly with a length of 17 mm on 3/8/24, remaining at this length for 54 days before fracturing to 20 mm on 26/9/24 and then to 36 mm on 8/10/24. Another fracture event to 51 mm occurred on 27/10/24, at which point the split started to grow continuously until 24/11/24, when it fractured again, and then continued to grow to reach a length of 153 mm on 30/12/24.

The split growth is characterised by abrupt increases due to fracture, and an increase in the growth rate as the split becomes longer. While there is a lack of published research on the development of longitudinal splits in uPVC pipes, this progression is consistent with what we know about fatigue fracture, evidence of crack growth marks on failed pipe samples and field work that identified the acoustic signals of minor fractures in pipes (allowing planned repairs to be conducted before catastrophic failure occurs).

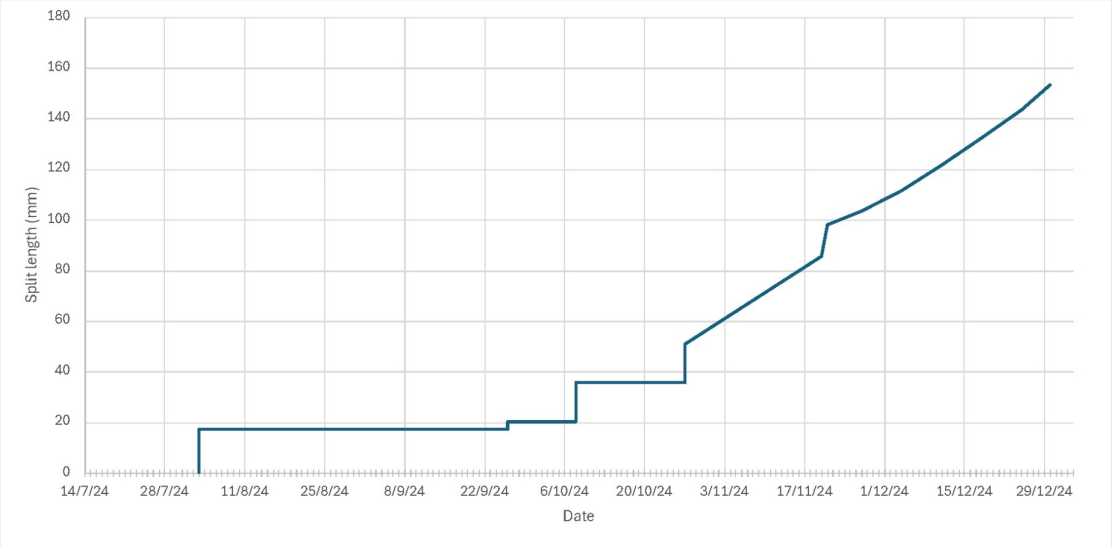

Figure 7 Estimated split length over time.

Finally, the progression of the split was calculated for two scenarios to evaluate the impact of assumptions on the results. Fig. 9 shows the progression of the split for an initial split width of zero and a split length of 100 mm. The scenarios develop to different final split lengths but follow a similar pattern.

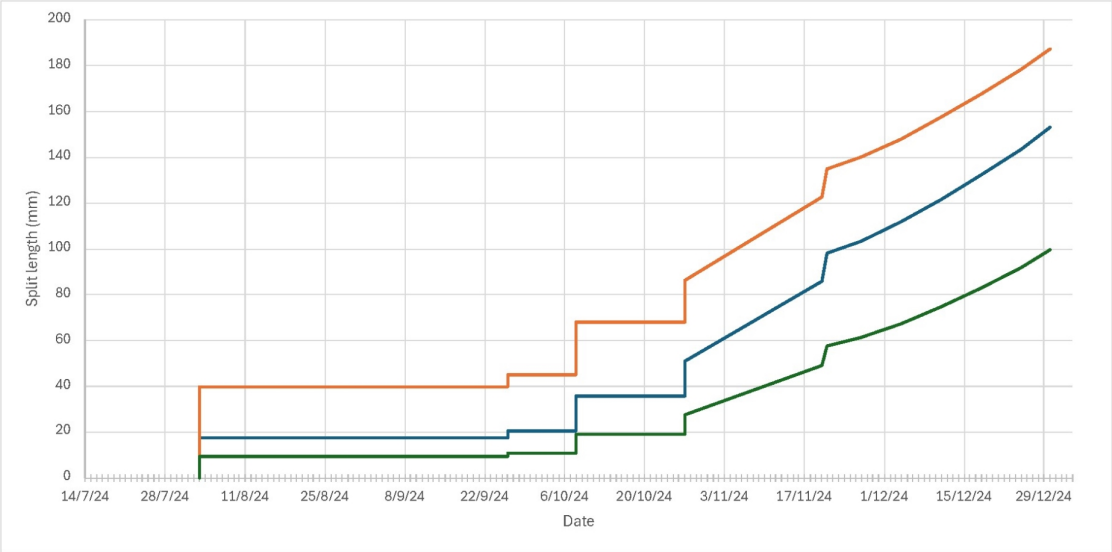

Figure 8 Progression of the split length for different model input parameters

3 Leak-Soil Interaction

3.1 Introduction

Soil and pipe hydraulics are very different. Pipe flow is associated with large pressure heads (20 – 100 m), turbulent flow, and high velocities. In contrast, at the depths where water pipes are typically buried (< 2 m), the pore pressure heads in fully saturated soils would be below 2 m, soil flow is usually laminar (Darcy flow), and average flow velocities are generally small (< 0.01 m/s).

When a leak, like the McCrae split, occurs in a pipe, the soil surrounding the pipe is exposed to a water jet moving at a very high velocity, estimated as 37 m/s in the case of McCrae (see Table 2).

There is an incompatibility between the pipe leak and soil flow capacities. In general, the interaction between a leaking pipe and its surrounding soil is complex due to the interaction of soil particles with the leakage jet, turbulent flow in the soil, changing geometry of the unconfined flow regime, hydraulic fracturing, and piping (Van Zyl and Clayton, 2013).

The stress conditions in the ground will contribute to how flow takes place. Calculations of Darcy flow generally assume permeability to be constant, with flow distributed across the entire region of permeable soil. Considerations of force equilibrium make it clear, however, that for a particulate material such as soil, the maximum water pressure in the pores between the particles, on any given plane, cannot exceed the (total) stress on that plane (Van Zyl and Clayton, 2013).

The total stress on a plane in a soil mass is the stress on that plane arising from external loading and the self-weight of the soil. This is distinct from effective stress, which governs the strength, compressibility, and, to some extent, soil permeability. It is also the numerical difference between total stress and pore pressure on any plane. Once the water pressure at any point in the ground rises above the minor total principal stress (which may be in the horizontal or vertical direction, but is unlikely to exceed 20–30 kPa (2 – 3 m) for typical pipe burial depths), hydraulic fracture takes place. The soil cracks along planes of weakness, flow occurs preferentially along these cracks, flow rates rise through orders of magnitude, and conventional seepage analysis is no longer applicable (Van Zyl and Clayton, 2013).

Even if the water pressure is not sufficiently high to cause hydraulic fracture, if upward flow occurs in unbonded granular soil and its velocity becomes sufficiently great, fluidisation to the surface may occur. This is known as 'piping' and results when the upward force on the soil particles resulting from seepage exceeds its buoyant self-weight, and occurs at a hydraulic gradient approximately equal to unity (Van Zyl and Clayton, 2013).

When a new leak is created, pressure will initially build up in the soil, leading to hydraulic fracture or lift of the soil's surface along a shear cone. This, in turn, will create space for soil particles near the leak to move, leading to local fluidisation.

3.2 Local Fluidisation

Fig. 9 shows local fluidisation occurring in a uniform bed of glass beads in a laboratory experiment (Bailey and Van Zyl, 2015). Three zones can be distinguished (Van Zyl et al., 2013):

- Fluidised zone. A high-velocity inner zone that is directed away from the leak and terminates in a vortex movement. It consists of water with soil particles suspended in it. The fluidised zone picks up soil particles from the mouth of the leak and deposits them at the terminating head.

- Mobile bed zone. The mobile bed zone surrounds the fluidised zone and is characterised by packed soil particles moving steadily from the terminating end of the fluidised zone to the leak outlet.
- Static bed zone. Outside the mobile bed zone, the soil remains stationary and unaffected by the water jet.

Local fluidisation of the soil outside the leak may cause scouring of the pipe wall surface, reducing the wall thickness and accelerating leak growth. Since the McCrae failed pipe section was not retained, it wasn't possible to inspect the surface for evidence of scour.

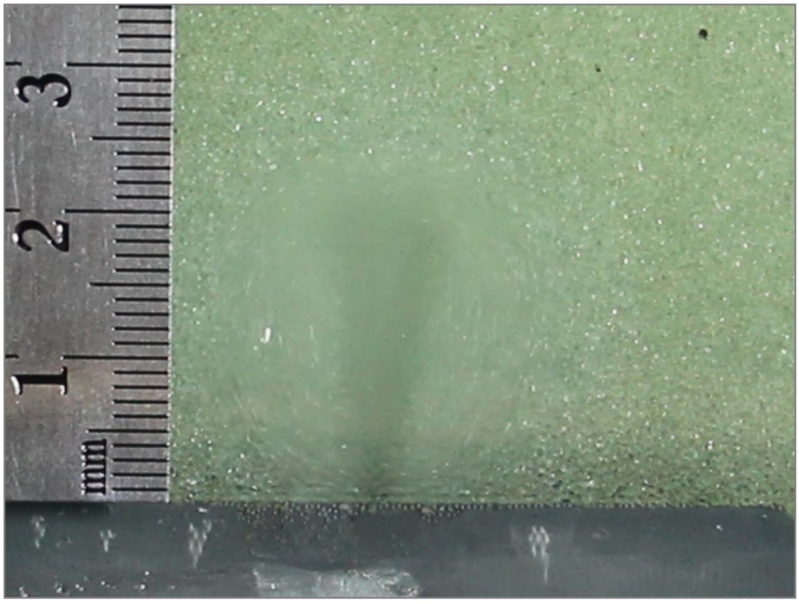

Figure 9 Local fluidisation in a uniform granular medium caused by a simulated leak through the bottom of the tank (Bailey, 2015)

3.3 Piping to the Soil Surface

It is possible that a stable local fluidisation zone developed outside the McCrae split in the early stages of the leak when the flow rate was low enough for the soil to absorb. However, as the split grew and the leakage flow rate increased, the pressure, velocities and extent of the fluidised zone would have increased.

Since the McCrae leak was located at 4 o'clock, the fluidised zone would not have been directed at the soil surface. However, it is likely that water would have preferentially moved along zones of higher permeability or lower resistance. Once the flow reached the soil surface, a flow path with lower resistance than the contained flow zones would have been created along which water would preferentially move. Once the flow velocity along this path reached a critical value, soil particles would have been washed away, further reducing the resistance to flow and reinforcing the process. This process could have led to the creation of a pipe through the soil, providing an unrestricted path for the water leaving the leak to reach the surface. Hydraulic fracture may also have played a role in creating this flow path.

4 Leakage Flow Reaching the Surface

4.1 Introduction and Assumptions

This section presents simplified analyses, with the aim of estimating the quantity of leakage flow reaching the surface (both in terms of daily leakage flow and as a proportion of daily leakage flow). The purpose of these simplified analyses is to provide comparative, order-of-magnitude estimates on where burst flow is likely to have been transmitted in the vicinity of the pipe (i.e. is it more likely that a majority of leakage flow travelled directly to the surface, or was a substantial portion of leakage flow transmitted through the soil and pipe bedding material). A number of simplifying assumptions were made in this analysis to allow estimates of volumetric flow rates to be performed using straightforward quantitative calculations. For the purposes of this analysis, the following flow mechanisms and simplifying assumptions were considered, as summarised below.

Flow directly to surface through an unrestricted flow channel: As described in Section 3, a portion of the burst flow was assumed to travel toward the ground surface in a zone of localised fluid flow, travelling directly from the pipe burst to the ground surface within a cylindrical channel. Within this zone, flow velocity was assumed to be constant across the cross-sectional area of flow, and the diameter of the flow zone was assumed to be constant between the pipe and the ground surface. The diameter of the area in which fluid flow occurred was assumed to be bounded by the diameter that would produce a flow velocity equivalent to the erosion velocity of the material, and by the channel diameter that would produce a flow velocity equivalent to the deposition velocity of the in-situ soil.

Flow within pipe bedding sand, in-situ soil, and sewer bedding sand/gravel. A portion of the flow was assumed to occur within the pipe bedding material, the in-situ soil, and potentially within the bedding material of a nearby sewer pipe. For these analyses, saturated flow was assumed, and Darcy's law was assumed to apply, with volumetric flow rate calculated using $Q = k\ i\ A$ (where Q = volumetric flow rate, k = permeability, i = hydraulic gradient, A = cross-sectional area). Where an assumption for soil permeability was required, permeability values were estimated on the upper end of typical ranges to account for preferential flow through defects at field scale (e.g. measured permeability for in-situ soil was approximately 10^{-7} cm/sec, but a permeability range of 10^{-5} cm/sec to 10^{-3} cm/sec was assumed for flow calculations). For flow calculations within pipe and sewer bedding material, a hydraulic gradient of i = 0.1 was assumed (equivalent to the grade of the sewer pipe). For downward flow calculations within in-situ soil between the pipe bedding material and the sewer bedding material, a hydraulic gradient of i = 1.0 was assumed. Flow within the in-situ soil beyond the pipe bedding material was assumed to be negligible (relative to potential flow within the pipe and sewer bedding material), due to the comparatively low permeabilities measured at a nearby borehole.

Proportion of leakage flow reaching the ground surface. To estimate the proportion of burst flow reaching the ground surface, it was assumed that the calculated volumetric flow rate within the pipe bedding material and sewer bedding material occurred at all times, regardless of burst flow volume (for cases where burst flow volume was less than the assumed flow capacity of the pipe and sewer bedding material, the proportion of the flow reaching the surface was assumed to be zero). For this analysis, any volumetric flow rate that exceeded the flow capacity of the pipe bedding material and surrounding soil was assumed to reach the ground surface.

Interaction between different flow pathways. The volumetric flow rates estimated herein have been analysed in terms of each proposed flow pathway's capacity to transmit flow, and interaction between various flow paths has not been modeled (e.g. the sewer bedding gravel is assumed to transmit flow at full capacity, despite the flow needing to travel through lower permeability zones to

reach the sewer bedding gravel).

4.2 Soil Properties

4.2.1 Soil Classification, Grain Size Distribution

Based on a borehole near the burst location (BH01) and a borehole at the nearby WR174 low-level storage site, the in-situ soil in the vicinity of the pipe burst appears to be predominantly residual and colluvium soils, consisting predominantly of sandy clay, silty clay, clayey sand, and silty sand. Soil particle size distribution tests performed on two samples indicate a well-graded material, with median particle sizes (D_{50}) of approximately 0.3 mm (corresponding to fine sand particles). D_{10} was approximately 0.01 mm (corresponding to silt particles), and D_{60} approximately 0.4mm (corresponding to sand particles). Refer to particle size distribution testing data (Figure 10).

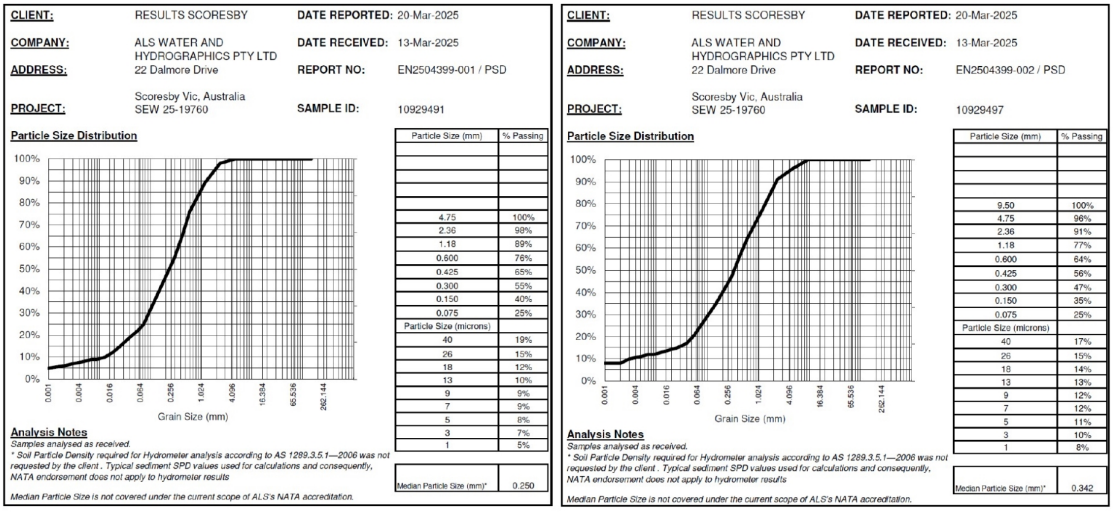

Figure 10 Soil Particle Size Distribution testing data.

4.2.2 Soil Profile and Subsurface Layering

Borehole data in the vicinity of the pipe burst (BH01) indicate colluvium and residual soils (sandy clay, silty clay, clayey silty sand, clayey sand, and sandy clay) in the vicinity of the pipe burst location, to depths of approximately 13.4m below the ground surface. Borehole data at the nearby WR174 low-level storage site indicate silty sand (SM) from the ground surface to depths of approximately 7.3m, with granite bedrock below 7.3m. Core photos of push tube samples from the upper 2.6m of soil at the WR174 site are shown below (Figure 11):

Figure 11 Sample photos from nearby borehole (WR174 low-level storage site)

4.2.3 Groundwater Conditions

Current assumptions are that the natural groundwater level in the vicinity of the pipe is at depth beyond the pipe location, rather than present near the ground surface (for this analysis, groundwater was assumed to be present at depth, rather than near the ground surface). During the installation of MW0227 at the nearby WR174 low-level storage site, groundwater observations during well development appear to support the assumption of a groundwater table at depth (rather than a shallow water table near the ground surface).

4.2.4 Soil Permeability

Typical permeability (k) for a silty sand (SM) is about 10^{-5} cm/sec to 10^{-3} cm/sec (Figure 12). Permeability values for typical colluvium and residual soils (sandy clay, silty clay, clayey silty sand, clayey sand, and sandy clay) are typically in the range of 10^{-7} cm/sec to 10^{-5} cm/sec (Figure 12). Permeability testing data for the nearby WR174 low-level storage site indicate the in-situ material has a measured permeability on the order of 10^{-7} cm/sec (10^{-9} m/sec), consistent with typical values for colluvium and residual soils. The pipe bedding material was assumed to consist of sand (typical k = 10^{-2} to 10^{-1} cm/sec), and the sewer bedding material was assumed to consist of gravel below the pipe (typical k = 10^{-1} to 1 cm/sec) and sand above the pipe (k = 10^{-2} to 10^{-1} cm/sec). For flow within the sewer bedding material, the composite permeability for the bedding material was assumed to be in the range of $5x10^{-2}$ cm/sec to $5x10^{-1}$ cm/sec (with a portion of the cross-sectional area consisting of sand, and a portion of the cross-sectional area consisting of gravel).

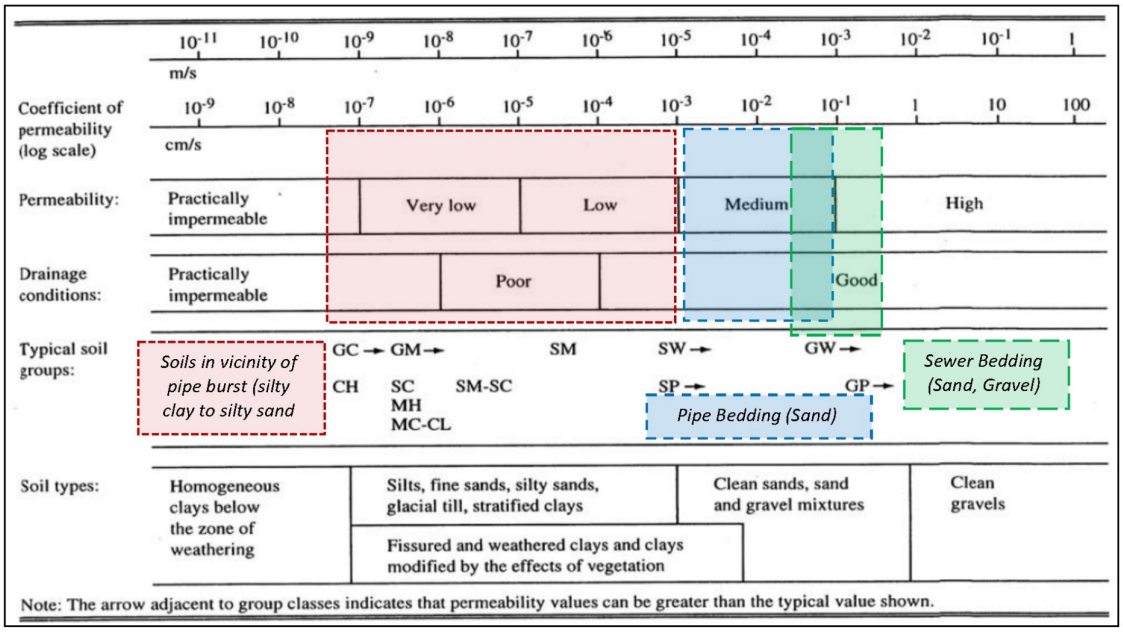

Figure 12 Typical permeability values in soil (FHWA-NHI-06-088, after Carter and Bentley, 1991)

4.2.5 Soil Erosion Velocity, Transport Velocity, Deposition Velocity

Based on the figure below (adapted from Hjulstrom, 1935), a soil with grain size ranges similar to those observed near the pipe would be expected to experience soil erosion at flow speeds above 20 cm/s (Figure 13). At flow velocities below approximately 0.7-2 cm/s, particles of 0.1-0.3 mm (equivalent to a fine sand) would be deposited. As particles of fine white sand were observed deposited along the ground surface near the burst location, it is assumed that the flow velocity

within the flow zone at a steady state would have been sufficiently slow to deposit fine sand particles, but sufficiently swift to transport silt and clay particles. For this analysis, it was assumed that erosion is triggered at velocities above 20cm/s, and that deposition occurs at flow velocities below approximately 1 cm/s.

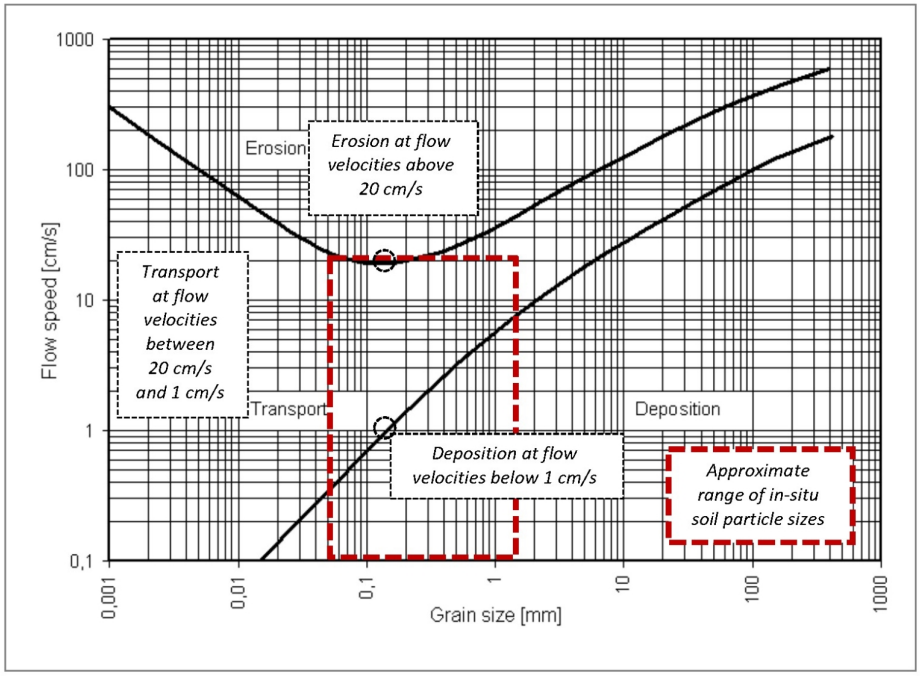

Figure 13 Hjulstrom diagram illustrating typical erosion, transport, and deposition velocities based on soil particle size (adapted from Hjulstrom, 1935)

4.3 Comparison of Site Observations with Estimates of Flow Pathways

4.3.1 Site Observations

4.3.1.1 Site Observations of Burst Area during Leak

Photos from the burst area appear to indicate the development of a localised zone of fluidisation and soil piping, through which water travelled to the ground surface. On 30/12/2024, a flow channel of approximately 300mm was observed, with a water spout emerging, surface water runoff, and no sign of undermining or cavity forming (Figure 14). This photo appears to indicate the development of a localised zone of fluidisation and soil piping. This zone would provide a conduit for most of the burst flow to reach the ground surface directly, with some infiltration and seepage into adjacent soils.

Figure 14 Site photo of burst flow zone, indicating development of a water spout and flow channel at the ground surface of approximately 300mm in diameter (photo date 20/12/2024).

4.3.1.2 Site Observations of Burst Area during Pumping/Dewatering

Photos taken during pumping/dewatering activities associated with burst repair appear to indicate some erosion/caving occurred near the ground surface during pumping, and the development of a roof (self-supporting zone of arched soil) as water and soil were removed, typical of saturated colluvium/residual soils similar to those observed on site (Figure 15). Photos indicate a potential zone of eroded soil of approximately 0.9m to 1.6m in diameter was observed during pumping (dimensions scaled from a fence near the burst zone).

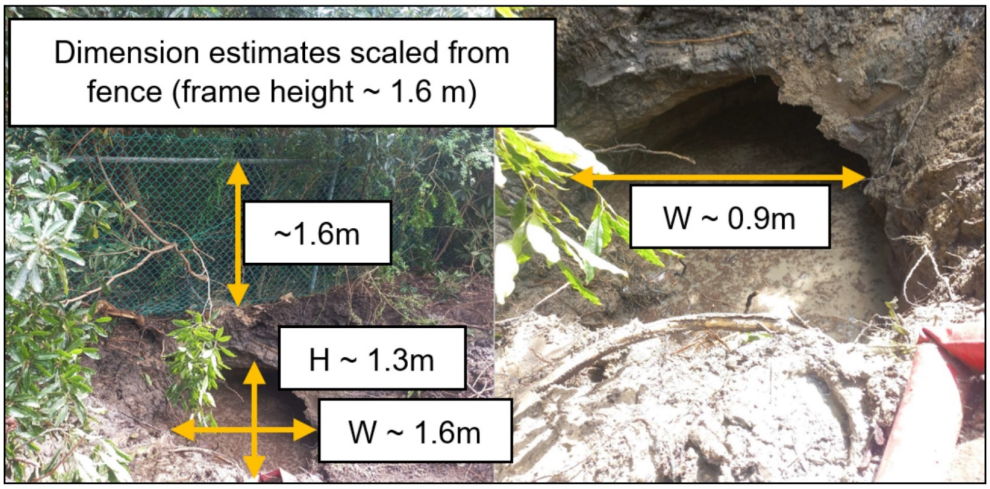

Figure 15 Site photos of erosion/caving observed during pumping/dewatering.

4.3.2 Site Observations of Soil Surrounding Pipe during Repair

Excavation photos from the pipe repair indicate relatively competent soil in the area adjacent to the pipe, suggesting a limited area of soil fluidisation in the zone around the pipe (Figure 16).

Figure 16 Site photos of the pipe repair area.

4.3.3 Proposed Mechanism for Burst Flow Reaching Surface

4.3.3.1 Development of Flow Channel between Burst and Ground Surface

Preliminary conceptual calculations indicated that a cylindrical flow channel within the soil with a diameter of between about 0.3m and 1.5m could pass about 1.5 ML/day with sufficient flow velocity to transport silty sand material (the lower diameter corresponds to the erosion velocity of 20 cm/sec, and the higher diameter to the assumed deposition velocity of 1 cm/sec). The proposed mechanism of flow reaching the ground surface is the development of a fluidised zone between the burst and ground surface, bounded by erosion velocity and deposition velocity (Figure 17).

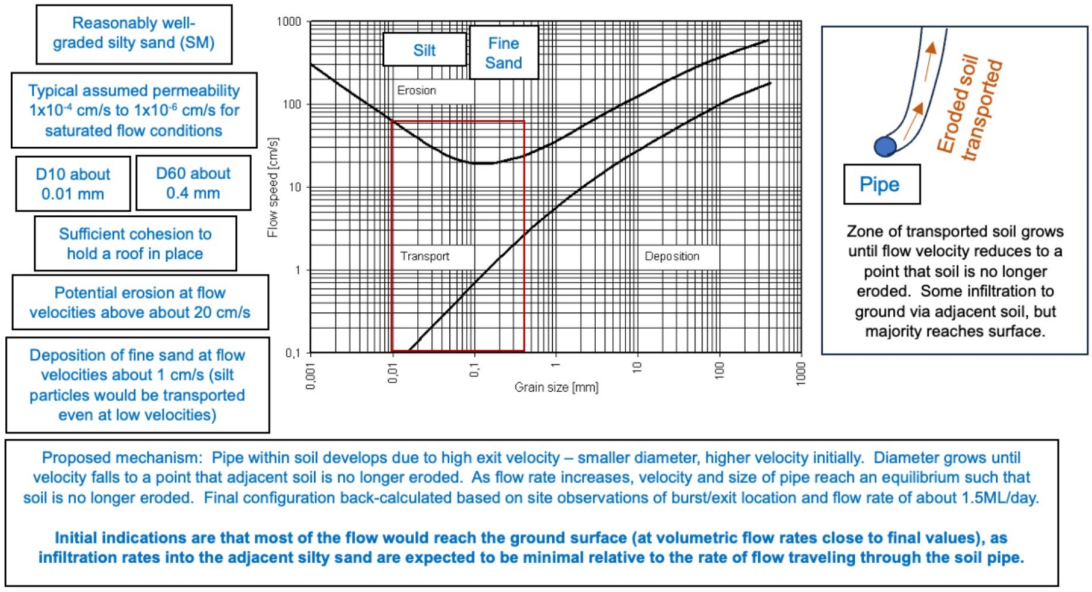

Figure 17 Annotated schematic of proposed burst flow mechanism (preliminary/conceptual version)

4.3.4 Geometry of Pipe and Sewer Bedding Material

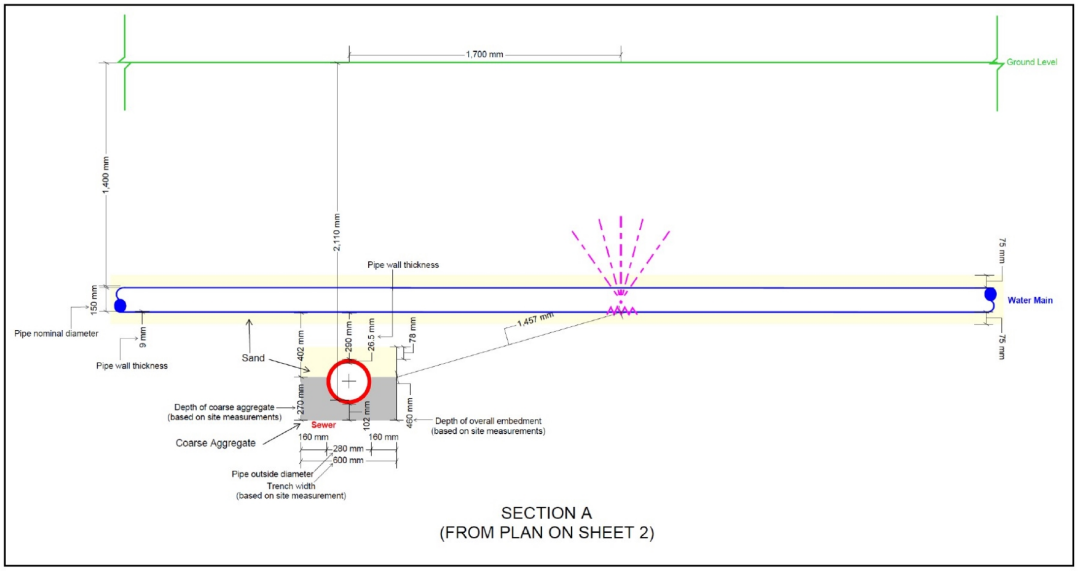

Figure 18 Sketch of pipe elevations in vicinity of the burst area.

4.4 Proposed Mechanisms of Burst Flow Pathways

The figure below (Figure 19) summarises proposed flow mechanisms for burst flow pathways, along with calculated flow rates for each form of flow (refer to previous sections for a discussion of simplifying assumptions associated with these estimates). Complete quantities are provided subsequently (Table 3).

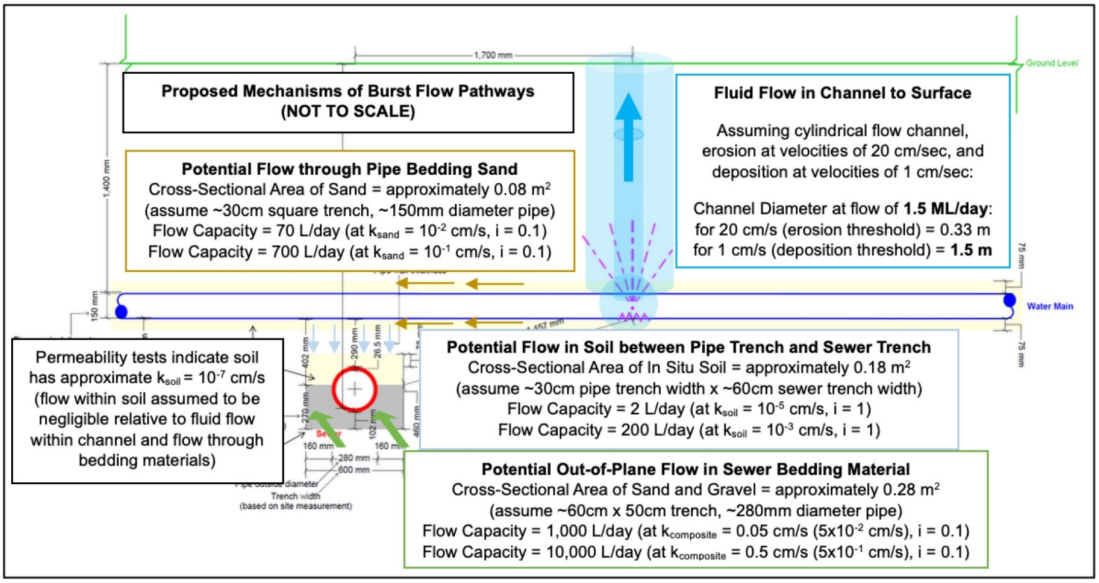

Figure 19 Annotated site sketch with proposed mechanisms of burst flow pathways and flow capacities

Sample calculation for cylindrical flow channel diameter at a flow rate of 1.5 ML/day:

Assumed flow velocity = 20 cm/sec = 0.2 m/sec (equivalent to flow velocity causing erosion)
Cross-sectional area of flow channel = A = $\pi \times D^2 / 4$
Volumetric flow rate = 1.5 ML / day x (m^3 / 1000 L) x (day / 86400 sec) = 0.017 m^3 / sec

Flow rate = Average Velocity x Cross-Sectional Area = 0.017 m^3/sec = 0.2 m/sec x ($\pi \times (D^2) / 4$)

Solve for Diameter, $D = \sqrt{\left(\frac{4 \cdot (Flow\ Rate)}{\pi \cdot (Flow\ Velocity)}\right)}$ = sqrt [(4 x 0.017 m^3/sec) / (π x 0.2 m/sec)] = **D = 0.33 m**

Sample calculation for sewer bedding material flow capacity:

Cross-sectional area (including pipe) = L x W = 0.6 m x 0.5 m = 0.3 m^2
Cross-sectional area of pipe (external) = $\pi \times D^2 / 4 = \pi \times (0.28\ m)^2 / 4$ = 0.06 m^2
Cross-sectional area available for flow = total area – pipe area = 0.3 m^2 – 0.06 m^2 = 0.24 m^2
Permeability of sand = assume $k_{sand} = 10^{-1}$ cm/sec = 10^{-3} m/sec
Permeability of gravel = assume $k_{gravel} = 1$ cm/sec = 10^{-2} m/sec
Composite permeability (assume 50% sand, 50% gravel) = $k_{composite} = 5x10^{-1}$ cm/sec = $5x10^{-3}$ m/sec

Assume hydraulic gradient = i = 1/10 = 0.1 (equal to grade of sewer pipe)

Flow rate (Darcy's Law) = Q = k i A = ($5x10^{-3}$ m/s) (0.1) (0.24 m^2) = 0.00012 m^3/sec

Flow rate = 0.00012 m^3/sec x 1000 L / m^3 x 86400 sec / day = 10,368 L / day ≈ **(10,000 L / day)**

Table 3 Estimates of Flow Capacity within Pipe Bedding, Sewer Bedding, and Soil Between Pipe and Sewer

Estimated Flow Capacity of Pipe Bedding Material	Parameter	Units	**Value**	**Value**
Approximate Permeability of Pipe Bedding Sand	k_{sand}	cm/sec	1.00E-02	1.00E-01
Approximate Width of Pipe Bedding Sand	W_{sand}	cm	31.8	31.8
Approximate Height of Pipe Bedding Sand	H_{sand}	cm	31.8	31.8
Approximate Diameter of Pipe	D_{pipe}	cm	16.8	16.8
Cross-Sectional Area of Sand + Pipe	A_{total}	m^2	0.101	0.101
Cross-Sectional Area of Sand Only	A_{sand}	m^2	0.079	0.079
Hydraulic Gradient in Pipe Sand (assume 1/10, equivalent to grade of sewer)	i_{sand}	--	0.1	0.1
Flow Capacity in Sand (Assume Flow Occurs Over Entire Cross-Sectional Area)	Q_{sand}	L / day	**68.2**	**682.2**
Value used for Approximations of Flow Reaching Surface	$Q_{pipebedding}$	**L / day**		**1,000**

Estimated Flow Capacity of Sewer Bedding Material			**Value**	**Value**
Approximate Composite Permeability of Sewer Bedding Sand and Gravel	$k_{sand\&gravel}$	cm/sec	5.00E-02	5.00E-01
Approximate Width of Sewer Bedding Sand and Gravel	$W_{sand\&gravel}$	cm	60	60
Approximate Height of Sewer Bedding Sand and Gravel	$H_{sand\&gravel}$	cm	46	46
Approximate Diameter of Sewer Pipe	$D_{sewerpipe}$	cm	28	28
Cross-Sectional Area of Sand and Gravel + Pipe	A_{total}	m^2	0.276	0.276
Cross-Sectional Area of Sand and Gravel Only	$A_{sand\&gravel}$	m^2	0.214	0.214
Hydraulic Gradient in Pipe Sand (assume 1/10, equivalent to grade of sewer)	$i_{sand\&gravel}$	--	0.1	0.1
Flow Capacity in Sand (Assume Flow Occurs Over Entire Cross-Sectional Area)	$Q_{sand\&gravel}$	L / day	**926.3**	**9263.2**
Value used for Approximations of Flow Reaching Surface	$Q_{sewerbedding}$	**L / day**		**10,000**

Estimated Flow Capacity of Soil Between Pipe Bedding and Sewer Bedding			**Value**	**Value**
Approximate Permeability of Soil Between Pipe Bedding and Sewer Bedding	k_{soil}	cm/sec	1.00E-05	1.00E-03
Approximate Width of Soil (Plan) Between Pipe Bedding and Sewer Bedding	W_{soil}	cm	31.8	31.8
Approximate Length of Soil (Plan) Between Pipe Bedding and Sewer Bedding	H_{soil}	cm	60	60
Cross-Sectional Area of Soil Between Pipe Bedding and Sewer Bedding	A_{total}	m^2	0.191	0.191
Hydraulic Gradient in Pipe Sand (assume 1 for downward vertical flow)	$i_{sand\&gravel}$	--	1	1
Flow Capacity in Sand (Assume Flow Occurs Over Entire Cross-Sectional Area)	$Q_{sand\&gravel}$	L / day	**1.6**	**164.9**
Value used for Approximations of Flow Reaching Surface	$Q_{soilbetweenpipe\&sewer}$	**L / day**	**negligible**	

4.5 Percentage and Volume of Flow Reaching Ground Surface

Based on the preceding analyses, and assuming flow rates of 1,000 L/day in the pipe bedding material and 10,000 L/day in the sewer bedding material, the following charts were developed (dates and flow rates estimated based on the modelled leakage flow rate versus time, **Error! Reference source not found.**). For the purposes of the following computation, seepage through the in-situ soil was assumed to be negligible relative to the flow capacities of the higher permeability bedding materials and the fluid flow channel developing between the pipe burst and ground surface (the assumption of relatively low seepage flow rates through the in-situ soil is supported by the measured permeability values). Quantities for selected dates are provided subsequently (Table 4).

In the figure below (Figure 20), the total flow volume reaching the surface and the percentage of flow volume reaching the surface were calculated as below (sample calculation shown for a flow rate of 1.4 ML/day or 1,400,000 L/day, equivalent to the modelled leakage volume on 30/12/2024):

$$Volume\ reaching\ surface = (Daily\ Flow\ Rate - Flow\ Capacity\ of\ Bedding\ Material)$$

$$= 1{,}400{,}000\frac{L}{day} - 1000\frac{L}{day} in\ pipe\ bedding - 10{,}000\frac{L}{day} in\ sewer\ bedding$$

= 1,389,000 L / day reaching the ground surface at a daily flow rate of 1.4 ML/day.

$$Proportion\ reaching\ surface = \frac{(Daily\ Flow\ Rate - Flow\ Capacity\ of\ Bedding\ Material)}{(Daily\ Flow\ Rate)}$$

$$= \frac{1{,}400{,}000\frac{L}{day} - 1000\frac{L}{day} in\ pipe\ bedding - 10{,}000\frac{L}{day} in\ sewer\ bedding}{1{,}400{,}000\ L/day}$$

= 0.992 or 99.2% of flow reaching the ground surface at a daily flow rate of 1.4 ML/day.

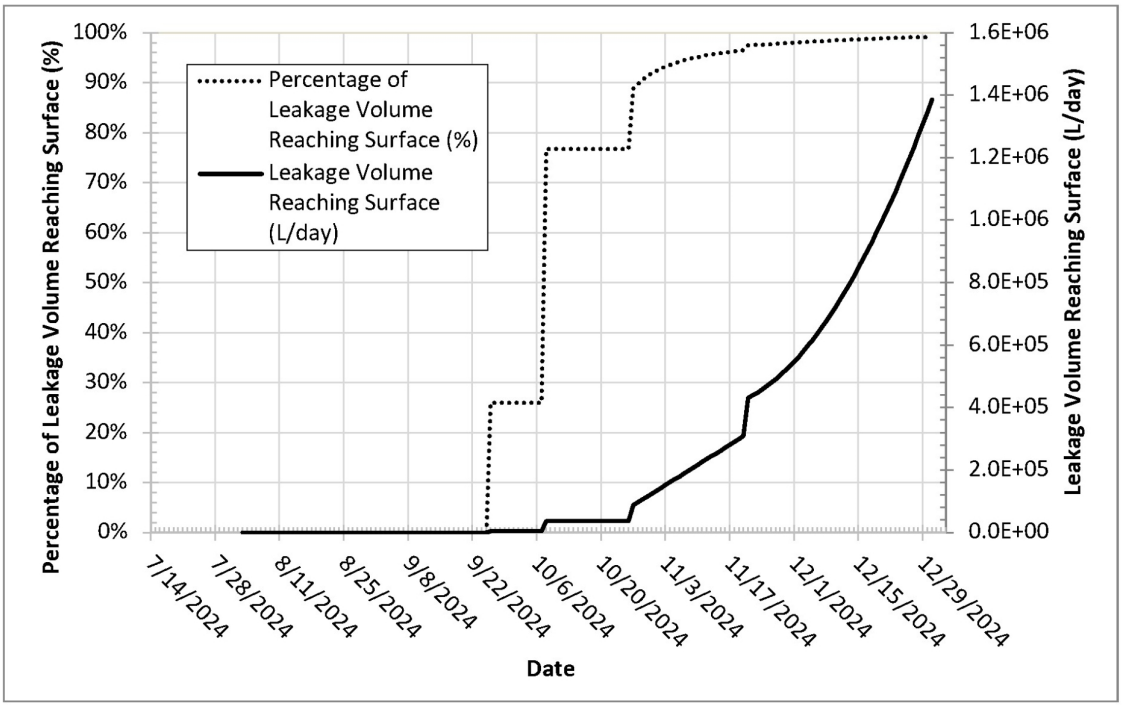

Figure 20 Proposed approximation of leakage volume and percentage of leakage volume reaching the surface versus time.

4.6 Development of Flow Channel with Time

Based on the calculation for flow channel diameter shown previously, the diameter of a cylindrical flow channel (between the pipe burst and the ground surface) can be estimated as the leakage volume increases with time. The development of a flow channel of increasing diameter with time is illustrated below (Figure 21). The channel diameter corresponding to the erosion velocity of 20 cm/sec appears to be consistent with site observations on 30/12/2024, which indicated a flow channel of approximately 300mm had developed in the vicinity of the burst zone, with a water spout emerging at ground surface, as illustrated previously in photos of the pipe burst area (Figure 14). Quantities for selected dates are provided subsequently (Table 4).

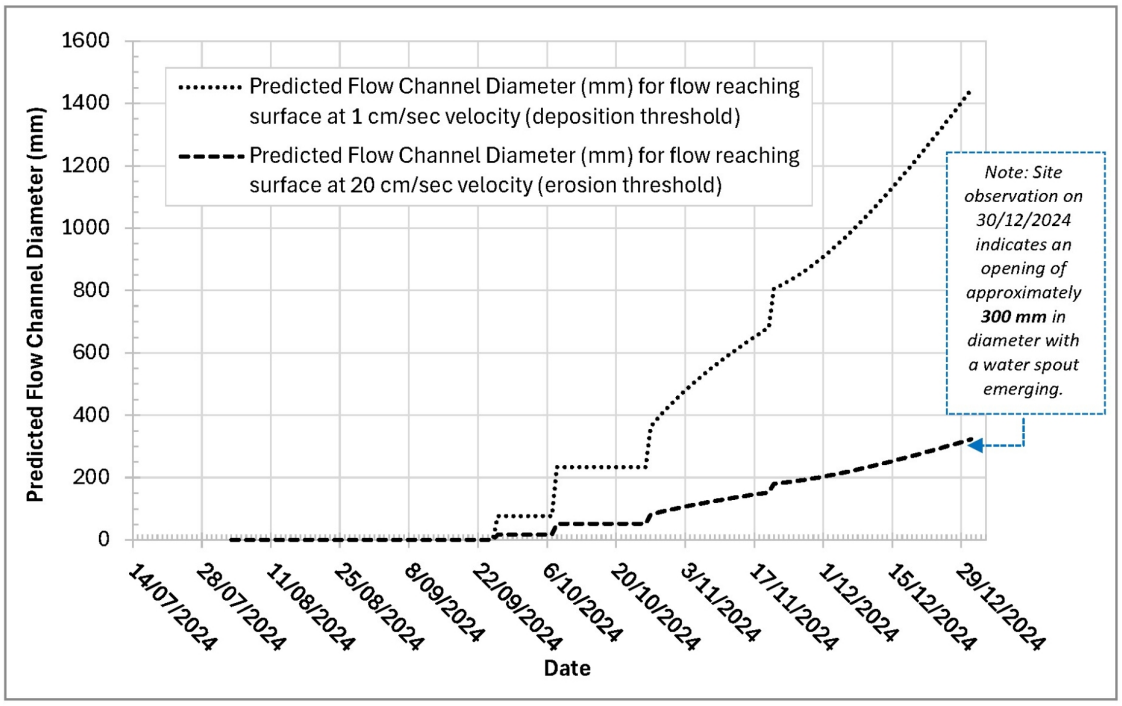

Figure 21 Proposed approximation of channel diameter versus time for flow reaching the surface.

Sample calculation for cylindrical flow channel diameter at a flow rate of 1.4 ML/day:

Assumed flow velocity = 20 cm/sec = 0.2 m/sec (equivalent to flow velocity causing erosion)
Cross-sectional area of flow channel = A = $\pi \times D^2 / 4$
Total volumetric flow rate = 1.4 ML / day x (m^3 / 1000 L) x (day / 86400 sec) = 0.016 m^3 / sec
Volume reaching surface = daily flow rate – flow capacity of bedding material
= 1,400,000 L/day – 1,000 L/day in pipe bedding – 10,000 L/day in sewer bedding = 1,389,000 L/day
Volume reaching surface = 1.39 ML / day x (m^3 / 1000 L) x (day / 86400 sec) = 0.016 m^3 / sec

Flow rate reaching surface = Average Velocity x Cross-Sectional Area
0.016 m^3/sec = 0.2 m/sec x ($\pi \times (D^2) / 4$)

Solve for Diameter, $D = \sqrt{\left(\frac{4 \cdot (Flow\ Rate)}{\pi \cdot (Flow\ Velocity)}\right)}$ = sqrt [(4 x 0.016 m^3/sec) / (π x 0.2 m/sec)] = **D = 0.32 m**

Based on the estimate above, at a flow velocity toward the surface of 20 cm per second (equivalent to the assumed erosion velocity), and a leakage flow of 1.4 ML/day (of which 1.39 ML/day reaches the surface), the predicted flow channel diameter would be approximately 0.32 m (320 mm).

Table 4 Estimates of Leakage Volume, Percentage of Leakage Volume Reaching Surface, and Predicted Flow Channel Diameters (Selected Dates)

Leakage Volume Reaching Surface, Percentage of Volume Reaching Surface, and Predicted Flow Channel Diameters (Selected Dates)					Flow Velocity for Diameter Calculation (cm/s)	
					20	1
Date	Modelled Leakage Volume (L/day)	Estimated Flow within Pipe and Sewer Bedding Materials (L/day)	Leakage Volume Reaching Surface (L/day)	Percentage of Leakage Volume Reaching Surface (%)	Predicted Flow Channel Diameter (mm) for flow reaching surface at 20 cm/sec velocity (erosion threshold)	Predicted Flow Channel Diameter (mm) for flow reaching surface at 1 cm/sec velocity (deposition threshold)
11/08/2024	10,891	11,000	-	0.0%	0	0
25/08/2024	10,891	11,000	-	0.0%	0	0
8/09/2024	10,891	11,000	-	0.0%	0	0
22/09/2024	10,891	11,000	-	0.0%	0	0
6/10/2024	14,867	11,000	3,867	26.0%	17	76
20/10/2024	47,297	11,000	36,297	76.7%	52	234
3/11/2024	163,300	11,000	152,300	93.3%	107	479
17/11/2024	292,123	11,000	281,123	96.2%	145	650
1/12/2024	558,843	11,000	547,843	98.0%	203	908
15/12/2024	858,676	11,000	847,676	98.7%	253	1129
20/12/2024	1,004,526	11,000	993,526	98.9%	273	1223
24/12/2024	1,135,896	11,000	1,124,896	99.0%	291	1301
27/12/2024	1,242,994	11,000	1,231,994	99.1%	304	1362
29/12/2024	1,318,473	11,000	1,307,473	99.2%	314	1403
30/12/2024	1,357,437	11,000	1,346,437	99.2%	318	1424
31/12/2024	1,397,217	11,000	1,386,217	99.2%	323	1444

4.7 Conclusions

Based on the preceding analyses, it appears that the majority of leakage flow travelled directly from the burst location to the surface via an eroded flow channel that developed within the soil (particularly as flow rates approached their peak values). This is supported by site observations, simplified calculations based on erosion and deposition velocity within the channel, and simplified estimates of flow capacities through adjacent soil and pipe bedding materials. In summary:

- At leakage flow rates of approximately 1.4 ML/day (equivalent to the maximum daily leakage volume), a cylindrical flow channel directly between the pipe burst and the ground surface was estimated to have a diameter of between approximately 0.3m (for a flow velocity sufficient to erode soil) and 1.5m (for a flow velocity sufficiently slow for soil to be deposited). This estimate appears consistent with site observations, which indicate a flow channel of approximately 300mm in diameter was observed on 30/12/2024, at a time near the of peak modelled leakage flow of 1.4 ML/day (a localised zone of erosion and caving of approximately 900mm to 1600mm in diameter was observed during site dewatering activities, although this zone may have developed during pumping/dewatering activities).
- Typical permeabilities for sand and gravel material were multiplied by cross-sectional areas of bedding material (excluding the pipe area) to examine the potential for flow within pipe bedding material. These approximate analyses indicate volumetric flow capacities of about 1,000 L/day in the water pipe bedding material and about 10,000 L/day in the sewer pipe bedding material (assuming saturated flow and hydraulic gradients of 0.1, equivalent to the grade of the sewer pipe). However, to reach the sewer pipe bedding material, the burst flow would need to travel through lower permeability zones, limiting the amount of burst flow that could reach the sewer bedding material.
- The simplified analyses shown here indicate that for leakage flow rates near the peak modelled value of approximately 1,400,000 L/day, the vast majority of the burst flow likely travelled directly from the burst location to the ground surface via a flow channel observed on site:
    - When sized according to flow velocities required for erosion and deposition, the capacity of a cylindrical flow channel directly between the burst location and the ground surface appears to be consistent with site observations near the time of peak flow rates of about 1.4 ML/day.
    - The capacity of in-situ soil to transmit high flow rates is limited due to its low measured permeability.
    - The capacity of pipe bedding to transmit flow is limited by cross-sectional area.
    - The capacity of the sewer bedding material to transmit flow is somewhat higher due to higher permeability bedding materials and a larger cross-sectional area, but peak flow capacity in the sewer bedding material (even if burst flow travelled directly into the sewer bedding material, and high permeabilities are assumed) would still be substantially less than the peak burst flow of 1.4 ML/day. Additionally, because the burst flow would need to travel through both the water pipe bedding material and the relatively impermeable in situ soil to reach the sewer bedding material, it is anticipated that flow rates within the sewer bedding material would be lower than the values indicated by fully-saturated flow.

Based on the preceding analyses, it is concluded that as leakage flow volume increased over time (particularly as flow rates approached their peak values in December 2024), the vast majority of the burst flow travelled directly to the ground surface via an eroded flow channel within the soil.

References

Bailey, N. D., & Van Zyl, J. E. (2015). Experimental Investigation of Internal Fluidisation Due to a Vertical Water Leak Jet in a Uniform Medium. In *Procedia Engineering* Vol. 119 (pp. 111-119).

Bardet, J. P., Ballantyne, D., Bell, G. E. C., Donnellan, A., Foster, S., Fu, T. S., List, J., Little, R. G., O'Rourke, T. D., and Palmer, M. C. (2010). Expert Review of Water System Pipeline Breaks in the City of Los Angeles during Summer 2009.

Barton, N. A., Farewell, T. S., Hallett, S. H., and Acland, T. F. (2019). "Improving pipe failure predictions: Factors affecting pipe failure in drinking water networks." Water Res., 164.

Beygi, S. and Van Zyl, J. E. (2024). Pilot study of the characteristics of different failure types in water distribution system pipes. *Journal of Pipeline Systems Engineering and Practice* **15**(3): 04024027.

Brandt, M. J., Johnson, K. M., Elphinston, A. J., and Ratnayaka, D. D. (2017). "Pipeline Design and Construction." Twort's Water Supply, 693–742. Elsevier.

Carter, M., and Bentley, S. P. (1991). Correlations of Soil Properties. Pentech Press Limited, London, U.K.

Cassa, A. M., and Van Zyl, J. E. (2013). "Predicting the pressure-leakage slope of cracks in pipes subject to elastic deformations." Journal of Water Supply: Research and Technology - AQUA, 62(4), 214-223.

Crook, J. (2025). McCrae Burst Volume - V4 250513_20250629.pdf, internal report.

ExcelPlas (2025), Report # 14028. Condition monitoring of a PVC pipe, ExcelPlas Polymer Technology and Testing, Moorabbin, VIC 3186, Australia

Farrow, J., Jesson, D., Mulheron, M., Nensi, T., and Smith, P. (2017). Achieving zero leakage by 2050: the basic mechanisms of bursts and leakage, UK Water Industry Res. Ltd., (Report Ref. No. 17/WM/08/60): 1–136.

FHWA (Federal Highway Administration) Soils and Foundations: Reference Manual. FHWA-NHI-06-088. Washington, D.C.: U.S. Department of Transportation, Federal Highway Administration, 2006. Soils and Foundations: Reference Manual. FHWA-NHI-06-088. Washington, D.C.: U.S. Department of Transportation, Federal Highway Administration, 2006.

Fox, S., Boxall, J. & Collins, R., 2018. Derivation and Validation of a Leakage Model for Longitudinal Slits in Polyethylene Pipes. *Journal of Hydraulic Engineering,* 144(7).

Hjulstrom, F. (1935). Studies of the morphological activity of rivers as illustrated by the River Fyris, Bulletin. Geological Institute Upsalsa, 25, 221-527.

Paris, P. C., & Tada, H. (1983). Application of fracture-proof design methods using tearing-instability theory to nuclear piping postulating circumferential through-wall cracks (No. NUREG/CR-3464). Del Research Corp., St. Louis, MO (USA).

Rajani, B., and Kleiner, Y. (2012). "Fatigue failure of large-diameter cast iron mains." Water Distrib. Syst. Anal. 2010 - Proc. 12th Int. Conf. WDSA 2010, 1146–1159.

Richard, H. A., and Sander, M. (2016). Fatigue Crack Growth: Detect—Assess—Avoid, Solid Mech. Its Appl.

Rooke, D. P., & Cartwright, D. J. (1976). Compendium of stress intensity factors.

Van Zyl, J.E., Alsaydalani, M.O.A., Clayton, C.R.I., Bird, T., and Dennis, A. (2013). "Soil fluidisation outside leaks in water distribution pipes – preliminary observations." *Proceedings of the Institution of Civil Engineers: Water Management*, **166**(WM10) 546-555.

Van Zyl, J.E., and Clayton, C.R.I. (2007). "The effect of pressure on leakage in water distribution systems." *Proceedings of the Institution of Civil Engineers: Water Management*, **160**(WM2) 109-114.

Van Zyl, J.E., and Malde, R. (2017). "Evaluating the pressure-leakage behaviour of leaks in water pipes." *Journal of Water Supply: Research and Technology – AQUA*, 66(5) 287-299.

Van Zyl, J. E., Lambert, A., and Collins, R. (2017). "Realistic modeling of leakage and intrusion flows through leak openings in pipes." Journal of Hydraulic Engineering, 143(9), 1-7.

Van Zyl, J.E., and Lin, Y.-T (2025). “Extensive experimental investigation of the pressure-leakage relationship in water pipes”, Journal of Hydraulic Engineering, Under review.